AD-A250 291

MENTATION PAGE

Form Approved
OMB No. 0704-0188

1. AGENCY USE ONLY (Leave blank)	2. REPORT DATE	3. REPORT TYPE AND DATES COVERED
	April 1992	Annual Report, 15 Dec 90 - 14 Dec 91

4. TITLE AND SUBTITLE (U)

Modeling Study to Evaluate the Ionic Mechanism of Soot Formation

5. FUNDING NUMBERS

PE - 61102F
PR - 2308
TA - A2
C - F49620-91-C-0021

6. AUTHOR(S)

H.F. Calcote, R.J. Gill, and C.H. Berman

7. PERFORMING ORGANIZATION NAME(S) AND ADDRESS(ES)

AeroChem Research Laboratories, Inc.
P.O. Box 12
Princton, NJ 08542

8. PERFORMING ORGANIZATION REPORT NUMBER

TP-508

AFOSR-TR- 92 0373

9. SPONSORING/MONITORING AGENCY NAME(S) AND ADDRESS(ES)

AFOSR/NA
Building 410
Bolling AFB DC 20332-6448

10. SPONSORING/MONITORING AGENCY REPORT NUMBER

11. SUPPLEMENTARY NOTES

12a. DISTRIBUTION/AVAILABILITY STATEMENT

Approved for public release; distribution is unlimited

12b. DISTRIBUTION CODE

13. ABSTRACT (Maximum 200 words)

It has been demonstrated that in a sooting laboratory flame the time to add a carbon atom to a growing carbon species is about the same, or shorter, for the ionic than for the free radical mechanism. The calculated step time is consistent with the experimentally observed time in the flame to build a soot particle. It has also been demonstrated that, up to about 30 carbon atoms, the thermodynamic driving force for the ionic mechanism is much greater than for the neutral mechanism; above 30 carbon atoms they are equal. The Langevin theory of ion-molecule reactions has been modified to accommodate large ions. The results indicate a greater collision coefficient for large ions than calculated by Langevin. The coefficient for a hard sphere collision decreases as ion diameter increases up to about 3 nm diam for a conducting spherical ion, and about 1 nm for a nonconducting spherical ion. The Sandia Flame Code has been modified to: (1) accept individual experimental concentration profiles as input; (2) use non-Arrhenius rate constants; and (3) accept ambipolar diffusion coefficients. Analysis of our previous modeling of the ionic mechanism and many runs with the modified code indicate either a basic flaw in the mechanism or a modeling problem. The detailed modeling results are inconsistent with the calculated speed with which carbon atoms are added and with the strong thermodynamic driving force for the ionic mechanism.

14. SUBJECT TERMS	15. NUMBER OF PAGES
Soot Formation; Ionic Mechanism; Thermodynamics; Ion-Molecule Reactions; Computer Modeling	37
	16. PRICE CODE

17. SECURITY CLASSIFICATION OF REPORT	18. SECURITY CLASSIFICATION OF THIS PAGE	19. SECURITY CLASSIFICATION OF ABSTRACT	20. LIMITATION OF ABSTRACT
Unclassified	Unclassified	Unclassified	UL

TP-508

TABLE OF CONTENTS

LIST OF FIGURES

TP-508

I. INTRODUCTION

This is the first annual report on a program to compare the ionic mechanism of soot formation with a free radical mechanism using computer modeling. In a previous contract[1] with the same objective we collaborated with Michael Frenklach and Hai Wang at Penn State.[2] In that program we developed the detailed chemical kinetic scheme, estimated the elementary reaction rates involved, and developed the thermodynamics of the ions involved in the ionic mechanism; this information had been unavailable. Frenklach and Wang improved the free radical mechanism and incorporated our ionic mechanism into the Sandia Flame Code which they used for the free radical mechanism. They ran the program on an IBM 3090 computer.

They experienced several problems in adapting the Sandia code to handle ions: (1) ionic diffusion, usually treated as ambipolar diffusion could not be incorporated into the code so an artificial fit was employed--this was accurate enough for these calculations, but was conceptually unpleasant; (2) non-Arrhenius ion-molecule reaction rate coefficients could not be accommodated by the code; and (3) experimental ion and neutral profiles could not be used as input to the code. The third limitation was the most serious because the program calculated excessive concentrations of small neutral species involved in the chemiionization steps and thus calculated too high concentrations of initial ions. It also had to carry along a large number of neutral species which made no contribution to the ionic mechanism and thus wasted the computer resources. These things limited our capability of evaluating the ionic mechanism, and the code predicted greater ion concentrations than would have been obtained were the neutral concentrations consistent with experimental data. Another major problem involved turnaround time; it usually took weeks to get a revised mechanism run, thus greatly limiting the number of computer experiments that could be performed.

To improve the situation, we hired Fokian Egolfopoulos (originally at Princeton University, now at the University of Southern California) to adapt the Sandia code to ions. He was very successful in this endeavor; the three above-mentioned problems were corrected. AeroChem purchased a Silicon Graphics workstation on which it installed the revised flame code. This operates very satisfactorily, with run times typically about 15 min to two hours and turnaround time instantaneous. This has allowed us to make more computer runs, whereby we have identified problems with the mechanism, or with the code, which were previously unsuspected.

During this report period we have, in addition to the above: (1) continued to expand the thermodynamic data base on ions[3]; (2) completed modifications to the Langevin theory of ion-molecule reactions to accommodate large ions (contrary to expectations the rate coefficients were increased); (3)

fine tuned the comparison between the free radical mechanism and the ionic mechanism by calculating the times to add a carbon atom to the growing species,[4,5] (the ionic mechanism appears to be faster); (4) compared the free radical mechanism with the ionic mechanism by determining the thermodynamic driving force between the two mechanisms (the driving force for the ionic mechanism is much greater); and (5) organized the experimental measurements made on benzene/oxygen flames under a previous contract[6] to form the experimental data base for comparing a computer model of the benzene/oxygen flame (this flame is much different from the acetylene/oxygen flame).

II. STATEMENT OF WORK

The ionic mechanism of soot formation in flames will be further evaluated and compared with the neutral mechanism by pursuing the following phases:

Phase I. Extend the Ionic Mechanism to Benzene-Oxygen Flames

1. Extend the thermodynamic and reaction rate coefficient data base to include those species found in benzene/oxygen flames which are not present in acetylene/oxygen flames.

2. Organize the experimental data available on the benzene flame including both neutral and ionic species.

3. Develop a detailed ionic mechanism for the formation of soot in benzene flames and submit this to others to run on a large computer to compare its agreement with experimental data and to compare its simulation of soot formation with the neutral mechanism.

4. Compare the computer modeling results with experimental data and interpret the results in terms of the major chemical pathway to soot in the benzene flame.

Phase II. Model Coagulation and Agglomeration

1. Extend the detailed mechanism of soot nucleation to include coagulation of large ions and neutrals, and charged with charged and neutral incipient particles.

2. Program a desktop computer to test the model developed in Task 1 (in a limited fashion) against experimental data. If warranted, submit this model to others to test on a mainframe computer.

3. Interpret the results from Task 2 in terms of a simplified mechanism.

Phase III. Develop a Theory for Large Ion-Molecule Reactions

1. Extend the Langevin theory of ion-molecule reactions to include large ions by removing the restriction of a point charge on the ion.

Phase IV. Compare Thermodynamic Predictions of Soot Formation with Experimental Observations

1. Collect and organize the literature data on soot yield and acetylene concentrations as a function of equivalence ratio.

2. Calculate the thermodynamic equilibrium concentration of acetylene and soot as a function of equivalence ratio for the literature systems identified in Task 1.

3. Compare the experimental and calculated values and interpret them in terms of generalizations relevant to the mechanisms of soot formation.

III. THERMODYNAMICS

Thermodynamic data continue to be developed for ions involved in the acetylene/oxygen flame. A paper[3] containing the thermodynamic data we have developed to date has been submitted to the Journal of Physical and Chemical Reference Data for publication. In the near future we will initiate collection and development of data on the oxygenated ions that appear in benzene flames but not in acetylene flames. This will be done in preparation for modeling the benzene/oxygen flame.

IV. REACTION MECHANISM AND REACTION COEFFICIENTS

The reaction mechanism and reaction rate coefficients previously reported[1] have been changed very little.

V. LANGEVIN THEORY FOR LARGE IONS

We have used the Langevin theory[7] to calculate ion-molecule reaction rate coefficients. This theory has repeatedly been shown to agree with experiments for small ions near room temperature, but has not been tested for large ions at flame temperatures. The theory assumes a point electric charge, which for large ions seems questionable. In Langevin's theory the collision rate constant is independent of molecular velocity, and thus temperature. However, more conventional neutral collision rates increase with temperature. The objective of the present study is to generalize the Langevin theory to account for ions of finite dimensions. The extension to finite dimensions results in a temperature dependence. A temperature effect has been investigated by Bei et al.[8] and others for small ions reacting with permanent dipole molecules, but the effect of temperature has not been demonstrated for nonpolar molecules and has not been studied for large ions.

Our work is being prepared for publication so it will be summarized here and some results given.*

Three ion models were studied. The first model considers the electronic charge to be at a point at the center of a nonconducting sphere of finite radius whose dielectric constant equals the vacuum value. Thus the electric field distribution is identical to Langevin's, but additional collisions are possible for faster relative speeds due to the physical size of the ion. This model is similar to that of Ref. 8.

The second model considers the ion to be a conducting sphere of finite radius. For this ion in free space the charge is uniformly distributed over the surface of the sphere. When polarizable neutral molecules are present, the neutrals become dipoles under the influence of the ion electric field, and they

*See Section IV for Nomenclature.

act to redistribute the ion's surface charge. This redistribution of the ion surface charge increases both the electric field strength at the neutral and its induced dipole moment.

The third model, "ion polarizability," considers the ion to be a nonconducting sphere of finite radius with the ionic charge in the center as in the first case, but with the capability of supporting an induced dipole moment at the sphere's center under the influence of an external electric field. A fourth approach would be to displace the charges making up the induced dipole within the sphere, but insufficient information is available to determine the displacement.

A. NONCONDUCTING SPHERE

A trajectory analysis using standard relationships for the electrostatic force on an induced molecular dipole leads to the following relation between the impact parameter b and the minimum separation distance between molecules that do not collide

$$\left[\frac{b}{r_{min}}\right]^2 = 1 + \frac{\gamma E(r_{min})}{\mu v_\infty^2} \tag{1}$$

In Langevin's theory a critical radius r_c exists for which $r > r_c$ corresponds to trajectories that do not lead to particle capture and $r < r_c$ corresponds to capture with r always decreasing monotonically to zero. The limiting case $r = r_c$ corresponds to orbital motion. In this case the electrostatic and centrifugal forces are balanced so that

$$\mu r\dot{\theta}^2 = -\gamma E\frac{dE}{dr} \tag{2}$$

Using the conservation of energy and angular momentum for the molecular trajectory and employing Eq. (2) leads to the following expression for r_c:

$$r_c E \frac{dE}{dr} + \frac{E^2}{2} = \frac{\mu v_\infty^2}{\gamma} \tag{3}$$

Equation (3) is the cornerstone of our analysis independent of the ionic model chosen. The assumption is that the induced dipole axis is always aligned with $\bar{r}$, the vector connecting the centers of the ion and the neutral molecule, throughout the trajectory from infinite radius to r_c. In our numerical computations the mean value of the three principal polarizability components for acetylene was used. The ratio of the mean to the minimum value is 1.187.[9]

Once an ion model is chosen one can calculate E and dE/dr as functions of r, and r_c is that value of r that satisfies Eq. (3) for a given value of v_∞ and neutral molecular properties. Setting $r_c = r_{min}$ in Eq. (1) results in a value for the impact parameter b in terms of the relative system kinetic energy at infinite separation. All trajectories with b less than this value will lead to collisions. Finally, the total collision rate k can be determined from

$$k = \pi \int v_\infty b^2 \frac{dn_v}{n} \tag{4}$$

with the Maxwell-Boltzmann distribution in kinetic energy used for dn_v/n.

This treatment is applicable to a nonconducting sphere. To this point there is no real difference between this formulation and Langevin's if Eq. (3) alone is used to find the impact parameter. However, Eq. (3) is not relevant when $r_c < a_i + a_n$, where a_i and a_n are, respectively, the ion and neutral molecule radii. In this case collisions occur at a given value of v_∞ for all impact parameters b less than that given by Eq. (1) with $r_{min} = a_i + a_n$.

Equation (4) is integrated in two kinetic energy ranges separated by the condition $r_c = a_i + a_n$. For the upper range of r_c the Langevin mechanism holds independent of the ion or neutral radii, but for smaller values of r_c there are additional collisions not included in the Langevin theory. This additional class of collisions becomes more important with increasing temperature. Even in this case the trajectories are still affected by the ion electric field so that the impact parameter is larger than for strictly neutral-neutral collisions.

B. CONDUCTING SPHERE

For the second ion model of a conducting sphere we determine the effect of a dipole on the sphere's surface charge distribution in terms of the simpler solution for an external point charge on a charged conducting sphere.

The classic problem[10] is that of a point charge of strength q_p external to a conducting sphere of radius a_i and total integrated surface charge q_i, the ionic charge. In the absence of an external charge the electric field can be represented by a point charge of strength q_i at the center of the sphere. With an external charge present an image method is used to construct the electric voltage potential field exterior to the sphere in terms of a simple distribution of point sources in the sphere. The external source induces an image source within the sphere located along a line joining the center of the sphere and the external point charge at a distance a_i^2/y from the center, where y is the distance from the center of the sphere to the external point charge. The charge of the image source is $a_i\, q_p/y$. To maintain the net ionic charge the value of the image charge is subtracted from the value of q_i at the sphere's center.

The electric field due to a dipole and a conducting sphere is obtained by superimposing the above solution for a positive point charge with that of a negative charge, displaced from the positive charge to form the dipole. The resulting field is quite different from that in Langevin's model when the dipole and sphere are close to each other. The field approaches infinity at a separation distance r_s which can be greater than the sum of the ion and molecule radii. With an infinite field a collision occurs independent of kinetic energy so that the equivalent hard sphere radius of the conducting spherical ion is greater than its physical radius.

In our computations Eqs. (3) and (1) and the new expressions for E are used with $r_{min} = r_c$ when $r_c > r_s$. When $r_c < r_s$, Eq. (1) is used to determine the impact parameter with $r_{min} = r_s$.

C. ION POLARIZABILITY

The third model considers the ion as well as the approaching neutral to be polarizable. Thus, the charge on the ion induces a dipole moment on the approaching neutral which in turn induces an electric field on the ion, inducing a dipole moment on the ion.

The polarizability of aromatic hydrocarbon ions has been studied[11] using molecular orbital theory and compared to data for naphthalene ($C_{10}H_8$). In this case polarizability for positive and negative ions is, respectively, within about 4 and 18% of the value for the neutral species. For our present study the

ion dipole will be assumed to be located at the center of the ion. It would be more realistic to have a charge distribution on the ion surface consistent with the dipole strength, but we have not attempted to model this.

Appropriate treatment leads to:

$$E_n = \frac{q_i}{x^2(1 - 4\gamma_i\gamma_n x^{-6})} \tag{5}$$

and this and its derivative are used in Eq. (3) to determine the impact parameter. Although it is possible for the denominator of Eq. (5) to be singular, we have not found this to be the case for the range of molecular parameters of interest.

With the electric field specified, the impact parameter is determined by Eqs. (1) and (3) when $r_c > a_i + a_n$ with $r_{min} = r_c$, and by Eq. (1) for $r_c < a_i + a_n$ with $r_{min} = a_i + a_n$. Integration over the Maxwell-Boltzmann distribution is split into two regions of velocity space to reflect the two different models of impact parameter.

D. RESULTS AND DISCUSSION

Results are shown in Fig. 1 for the ratio of the expanded Langevin collision rate, k_{EL}, calculated as above, to the Langevin collision rate, k_L, as a function of temperature for the conducting sphere and nonconducting sphere cases. The neutral molecule is assumed to be acetylene, and the ion is considered to be a sphere with a density of 1.5 g/cm^3. Curves are shown for ion diameters of 0.5, 1, and 2 nm.

It is seen in Fig. 1 that the collision rate for the expanded Langevin theory is increased by about five over the Langevin rate for the 2 nm nonconducting ion at typical flame temperatures. The conducting sphere case leads to an additional increase by nearly a factor of 2. The general increase with temperature is due to the finite size of the ions presenting a hard sphere cross-section.

This latter effect is illustrated in Fig. 2 in which the ratio of calculated collision rate to hard sphere collision rate is plotted as a function of temperature. There is little dependence on temperature at higher temperatures; the temperature effect is less for the larger ions. In particular, the 2 nm nonconducting case is very close to the hard sphere neutral-neutral collision value at all temperatures.

The effect of the ion diameter on the ratio of the expanded Langevin rate to the hard sphere rate is shown in Fig. 3. As the diameter increases, the enhanced rate coefficient due to an electric charge becomes less.

The third case, of an induced dipole in the ion, is not shown because the data differed little from the nonconducting sphere case, even for the lowest temperatures considered. The reason is that the dipole is assumed to be located at the sphere's center so that the separated ionic dipole charges cannot get very close to the neutral molecule dipole. Note that the x^{-6} dependence in Eq. (5) typical of dipole-dipole interactions, means that the effect falls off very rapidly with distance. If this case were modeled with a finite charge separation, the effect would be much larger.

In this study we have looked at generalizations of the Langevin theory. An important consideration not treated is that of geometry since large polycyclic aromatic hydrocarbons are often in the form of disks rather than spheres as assumed here. For example, the collision rate for a disk having the same mass as a sphere can be much greater than the sphere's rate due to the increase in surface area. This is easily shown by taking the rate k_s for a sphere to be:

$$k_s = \pi a_s^2 v_m \tag{6}$$

where a_s is the sphere radius and v_m is the mean molecular speed. For a disk of radius a_d, considering only collisions with the flat sides and not the edge, the sum of the collision rates k_d for both sides of the disk is:

$$k_d = \frac{\pi}{2} a_d^2 v_m \tag{7}$$

If the disk has a thickness h, then equating the volumes of the sphere and disk leads to

$$\frac{k_d}{k_s} = \frac{2}{3}\frac{a_s}{h} \tag{8}$$

or

$$\frac{k_d}{k_s} = \frac{2}{3}\left[\frac{3}{4}\right]^{1/3}\left[\frac{a_d}{h}\right]^{2/3} \tag{9}$$

Extending the analysis to compute the electric field of nonspherical ions, e.g., conducting and nonconducting prolate spheroids and disks is possible.[12] However, the trajectory analysis would be much more complex.

Other considerations are to use a fixed dielectric constant for the ion, which should yield results intermediate to those of the conducting and nonconducting cases, and to consider an off center location for the net ionic charge. These ideas can be extended to the nonspherical cases as well.

In summary, we have shown that treatment of finite size ions leads to collision rates in excess of those predicted by classical Langevin theory. The direction of future work in this area will be guided by our ability to model the significant structural and electrical properties of large hydrocarbon ions. This analysis has not yet been incorporated into the mechanism.

VI. COMPUTER MODEL

In our previous work our model was run on an IBM 3090 computer by M. Frenklach and Hai Wang at Penn State.[2] There was a long turnaround time and their code was not adaptable to ions or some of the computer tests which we wanted to do. We thus hired Fokian Egolfopoulos at Princeton University (now at University of Southern California) as a consultant to modify the flame code package, based on Sandia's CHEMKIN and Flame Codes. Modifications were made in the code to incorporate: (1) ion chemistry; (2) ambipolar diffusion of ions; (3) the ability to input neutral and ion profiles; and (4) the ability to employ a modified Arrhenius form for entering forward rate coefficients.

The modifications to include ambipolar diffusion coefficients replace the previous technique of using neutral diffusion coefficients of similar sized molecules. Brown in his treatment,[1] used Poisson's equation, which is the more correct way to account for diffusion. In addition, the revised code incorporates a charge neutrality check. Providing for incorporation of ion or neutral species profiles in the code allows us to employ as input experimental ion concentration profiles for several initial species (we have thus far used only one ion), and experimental concentration profiles for neutral species profiles

important in the ionic mechanism. This is similar to the frequently used technique of inputing experimental temperature profiles as data. It overcomes two problems previously experienced when evaluating the ionic mechanism. First we had to include the neutral species mechanism for small species to account for the production of chemiions. Thus we originally included about 40 neutral species and about 200 reactions from the neutral mechanism of soot formation. This added to the complexity of the program and increased computation time. The second problem was that the neutral mechanism produced an excess of chemiions over the experimentally observed quantities. We were thus biasing the ionic mechanism and were not testing the ionic mechanism alone but rather a combination of the ionic mechanism and the neutral mechanism. By using experimental data as input we can more accurately test the ionic mechanism.

In the present model, the ion-molecule reaction rate coefficients in the forward direction are fixed so that the equilibrium constant of the reverse reaction never exceeds the Langevin rate. When the free energy of the reaction changes sign through the temperature range of importance this is not straightforward. Therefore a modified Arrhenius rate coefficient equation was added to the flame code to accomplish this. This was done by making the forward rate coefficients for those reactions:

$$k = A \times T^n \times \exp(-E_{act}/RT) + B \qquad (10)$$

The constants: A, B, E_{act}, and B are determined empirically by fitting Eq. (10) to a curve of the forward rate plotted against the temperature, maintaining either the forward or reverse rate at the Langevin rate via the equilibrium constant. The computer code had to be modified to accept Eq. (10).

To test the computer models, AeroChem purchased a Silicon Graphics IRIS workstation. Run times have been relatively short, from a few minutes to several hours.

VII. COMPARISON OF CALCULATED AND EXPERIMENTAL ION CONCENTRATION PROFILES

The availability of the modified Sandia flame code to handle ions and the availability of a workstation have greatly accelerated the rate of progress on this program. As already implied, some of this seems to be in the wrong direction. There are several problems. Thermodynamic equilibrium seems

to have a much greater effect on the ion-molecule reactions than expected (the reverse reactions are calculated from the forward rate and the equilibrium constant); this shows up as a stronger temperature dependence than anticipated. At higher temperatures the ion-molecule reverse reactions become more important because entropy effects become more important with increasing temperature:

$$\Delta G_f = \Delta H_f - T\Delta S_f \tag{11}$$

This same effect, of course, controls neutral mechanisms and may very well explain why the rate of soot formation peaks in the temperature range of 1400 to 1900 K (see, e.g., Ref. 13). The usual explanation involves a competition between the rate of soot formation and the rate of soot oxidation.

The abnormal temperature effect on ion formation has shown up in several ways. In some of our first computer runs with Frenklach and Wang, a table with the experimental flame temperature vs. distance, in which one point was in error, was inadvertently used as input. This showed up in the calculation of ion profiles as a dip in the concentration profiles. In the ion profile calculations made by Frenklach and Wang, the ions always peaked much closer to the burner than the experimental data, see e.g., Fig 4; however, the maximum calculated concentrations were very close to the experimental maxima. We now interpret this as a combination of the temperature effect (the temperature is lower in the early part of the flame) and the use of calculated rather than experimental neutral species profiles in the ionic mechanism. We currently use experimental concentration profiles for those species which enter into the ionic mechanism. Using Brown's code,[1] the ions peaked at the appropriate distance, but the concentrations were far lower than measured. We do not know why the temperature effect did not show up here.

The difference between the measured ion and neutral species used as input data in our modified code runs compared with the calculated $C_3H_3^+$ ion and neutral species profiles is shown in Figs. 5 to 7. The calculated reactive linear propargyl ion, $C_3H_3^+(l)$ and experimental $C_3H_3^+$ maximum concentrations are reasonably close, Fig. 5, but at 0.5 cm above the burner, the calculated value is about an order of magnitude too high. It would be more reasonable to compare the cyclopropenylium ion, $C_3H_3(c)$, with experiment; now the calculated value is more than two orders of magnitude greater than the experimental value at e.g., 0.5 cm. Most of the neutral species are not too different, Figs. 6 and 7, but two reactive neutrals, C_4H_2 and C_4H_3 are different by about an order of magnitude at 0.5 cm, in opposite directions.

In our initial computer runs, employing as input data the experimental concentration profiles displayed in Figs. 5 to 7, we observed even less agreement with experiment, which we ascribe to temperature (equilibrium) effects, Fig. 8. In the calculated ion profiles, a first peak appears far closer to the burner than is realistic, but second, smaller, peaks are at approximately the correct position. Our working hypothesis is that this is a thermodynamic temperature effect. One possible explanation is that the ion-molecule reactions have an activation energy; such reactions usually do not have activation energies. If we assume activation energies between 80 and 250 kJ/mol these primary peaks can be made to disappear or become fairly small. Small peaks in ion concentration profiles have been observed near the burner experimentally[14,15]; the above temperature effect may explain that dilemma.

We ask why the thermodynamics, which controls the reverse reaction rates, plays such an important role. This effect seems to be even greater for neutral reactions.[4,5] We also ask why the calculated concentrations are so much smaller than the measured concentrations. It could, of course, be that ion growth is not the source of larger ions in flames, but, we have eliminated many other mechanisms.[4,16] Homann and associates[17] seem to be coming around to recognizing that the source of ions is ion growth as we proposed years ago![18] Maybe the experiments are off. It is difficult to see how they could be off by this amount. Equivalent experimental results have been obtained by Homann and associates in Germany[19,20] and by Delfau and associates in France.[21] We have not yet incorporated the results of the modified Langevin theory, but we do not anticipate that the changes will be sufficient to bring the experimental and calculated concentrations together.

Several rather "brutal" modifications have been made in an attempt to determine what has to be done to obtain agreement. We are now examining these in more detail to determine which are reasonable and which are nonsense. Clearly at some point, if we cannot obtain agreement with reasonable assumptions, we may have to abandon the concept that large ions grow from chemiions. This would obviously lead to the conclusion that ions have nothing to do with soot formation. A means of explaining the concentrations of large ions will then have to be developed. Because of the present situation, we will reexamine some of the proposed sources of large ions which we have previously reviewed and found wanting. From the standpoint of understanding the mechanism of soot formation, the removal of the ionic mechanism from the arena does not mean that current free radical mechanisms are to be accepted by default. Closer examination of the free radical mechanisms seems to lead to the same problems; the models do not agree with experiment.[4] As pointed out previously,[4] the free radical mechanisms do not predict the neutral species that are observed in flames, and when they do, they predict concentrations more than an order of magnitude too small for fairly small polycyclic aromatic hydrocarbons.

The results of the brutal modifications to the mechanism were not expected, e.g., reducing the ion recombination rate had no effect on the profiles! Further examination of this set of results, and

previous results, has given us some concern as to whether the computer code is appropriately handling the idiosyncratic requirements of ions. For example, the results of the detailed computer modeling are inconsistent with conclusions from calculating the time to add a carbon atom to the growing species[4] and the strong thermodynamic driving force for the ionic mechanism, see Section IX.

We are now checking the code to determine whether or not it is appropriately treating ions and whether we are using it correctly, and we are working toward making the above assumptions more reasonable. This will involve step by step analysis of the mechanism to identify the problem areas. We will also evaluate the use of more neutral reactants in the growth mechanism, especially C_3H_4, which in some reaction steps has been observed to be important. Toward simplification, we have based most of the mechanism on acetylene because the maximum concentration of acetylene is about 20 times greater than the maximum concentration of diacetylene, the next largest concentration of reactive species, and 700 times greater than the concentration of allene. When the reacting ion concentration is large, reaction with C_4H_2 or C_3H_4 in an exothermic reaction may be a better path than reacting with C_2H_2 in an endothermic reaction.

VIII. COMPARISON OF THE RATE OF CARBON SPECIES GROWTH FOR THE FREE RADICAL AND IONIC MECHANISMS

In the final report on the last contract,[1] we compared the rate of increase in carbon content by a free radical and the ionic mechanism, using experimentally measured neutral and ion species, and the appropriate rate coefficients. That comparison has been further tuned and has been submitted for publication.[4] When the more relevant experimental data of Bittner and Howard[22] are used rather than the data of Vovelle[23] (our burner and conditions were designed to match those of Bittner and Howard so such comparisons could be made) the ionic mechanism wins; compare 6.7 μs for the ionic mechanism with 25 μs for the free radical mechanism. This is still not persuasive, recognizing the inaccuracies in the data and in the rate coefficients, but it certainly demands attention.

The experimental data on which this analysis was made are presented in Fig. 9. To the extent that Bittner and Howard's data can be extrapolated to beyond 250 u, the ion and neutral concentrations become equal and the difference in growth rate will be determined by: the relative reaction rate coefficients; the concentration of the other reactants-- hydrogen atoms and acetylene for the free radical mechanism, and acetylene for the ionic mechanism; and the number of reaction steps to account for the same number of carbon atoms added, ratio 2/1 for the free radical mechanism over the ionic mechanism.

It is becoming increasingly difficult to defend a free radical mechanism against an ionic mechanism.

IX. COMPARISON OF THE THERMODYNAMIC DRIVING FORCE FOR THE IONIC AND FREE RADICAL MECHANISMS

The ultimate driving force for any sequence of chemical reactions, such as must occur for soot formation, is thermodynamics. As water flows downhill, reactions proceed in the direction of a negative gradient in free energy. To compare this driving force for ions, free radicals, and neutral molecules, we compare the free energy of formation of these three components of the ionic and free radical mechanism of soot formation in Figs. 10 and 11 for the two temperatures, 1000 and 2000 K.

Several features are obvious on inspection. First, the driving force for ions is distinctly greater than for free radicals or neutral molecules. Second, the free energy per carbon atom of either a free radical, a neutral molecule, or an ion rapidly levels off as the compound becomes larger. Third, the ion and neutral species free energies of formation converge when the species contain about 30 carbon atoms, i.e., a molecular weight of about 350 to 400 u.

The conclusions to be drawn are clear. There is very little thermodynamic driving force for the growth of free radicals or neutral molecules compared to the driving force for ions.

X. IONS IN BENZENE/OXYGEN FLAMES

In a previous program,[6] we measured ion spectra of benzene/oxygen flames in the same flames and on the same burner as used by Bittner and Howard[22] to measure neutral species profiles. This was done to have a data base for some day modeling that flame. We are currently analyzing that data in preparation for modeling the benzene/oxygen flame. Some of that analysis was presented at the Eastern States Section Meeting of the Combustion Institute.[24]

Several classes of ions can be distinguished on the basis of their profile shapes. $C_3H_3^+$ is assumed to be the primary ion. In both nonsooting (ϕ = 1.8) and sooting (ϕ = 2.0) flames, it exhibits

two peaks, a small one near the burner and a relatively large second peak downstream. It slowly decays further from the burner. The unique feature of the benzene flame is that a large number of oxygenated ions, e.g., $C_6H_7O^+$, are observed which are not observed in acetylene/oxygen flames. Most of the ions observed in acetylene/oxygen flames are also observed in the benzene/oxygen flame.

The apparent stability of the $C_3H_3^+$ ion in the benzene flame contrasts with its behavior in the C_2H_2/O_2 flame. In the benzene flame its concentration is an order of magnitude greater than the concentration of other ions; in the sooting acetylene flame it has the same order of magnitude concentration. In the benzene flames it decays more slowly than in the acetylene flame. The difference can probably be explained by the equilibrium between the linear reactive ion and the stable cyclic nonreactive ion favoring the nonreactive form at the lower temperature in the benzene flame compared to the acetylene flame. Some of the differences are probably due to the fact that the acetylene flame was more fuel rich, relative to the equivalence ratio for soot formation, than the benzene flames. Since the total ion concentrations in the benzene flames are greater than that in the acetylene flame, compare about 10^{11} with 7×10^9 ions cm^{-3}, the stability of $C_3H_3^+$ (cyclic) apparently does not limit the formation of large ions, but spreads their formation out over a greater distance. These differences between the two flames will hopefully be explained by the models.

Recently Löffler and Homann[25,26] reported ion profile measurements in sooting benzene/oxygen flames. The conditions in their experiments and in ours are compared in Table I. In Table II we compare the ions observed in acetylene/oxygen and benzene/oxygen flames and the ions observed at AeroChem and at Darmstadt in both flames. Löffler and Homann concentrate in their paper on oxygenated ions, but report observed spectra in Löffler's thesis. We have thus used these spectra to determine other ions observed in their flames.

In any such comparison of ions, or mass spectrometer data, one should be aware that the choice of the appearance of an ion contains a somewhat subjective factor in choosing which peaks to identify as important, and an objective factor that is dependent upon the sensitivity and resolution of the mass spectrometer. The list used here for acetylene/oxygen flames at Darmstadt was kindly furnished by Homann[28] to supplement those given in the paper.[19] Many other ions were identified by Homann; we used only those identified as "prominent peaks". Some of these ions, e.g., 71, 83, and 85 u are identified by Gerhardt and Homann in the acetylene flame as an oxygen molecule attached to an ion. This indicates reactions in the sampling cone of their instrument; these ions would not be expected to be stable in a flame. Our experience has been that the attachment of water, sometimes more than one water molecule, to an ion indicates sampling cone problems. Such ions can be gotten rid of by changing the cone structure, temperature, voltage, or pressure behind the cone. Some of their oxygenated species may in

fact be water clustered to an ion, e.g., 47, 67, 69, 71, 73, 83, 85, 95, 105, 109, and 119. This could be the case for some of the oxygenated species observed in both laboratories in benzene flames.

The above consideration raises again[29] the sampling problem of ions which have very high reaction rate coefficients. Are the identified ions the true ion or an ion that has been produced in the sampling system, by e.g., reacting with a species in large concentration, e.g., H_2O, as discussed above, or H_2, or $H\cdot$, or C_2H_2? This tends to muddle an already complicated problem. It means that the ion in the mechanism should, in some instances, be one that can simply, in an elementary reaction, produce the observed ion. This may, in fact, shed some light on the problems we are experiencing with computer modeling the mechanism, Section VI.

In general, for the benzene flame, Table II, the agreement in observed ions between Löffler and Homann and AeroChem are consistent, except for $C_{13}H_9^+$. We observe this ion but they do not. This is a very stable ion and we both observe it in large concentrations in acetylene flames. Instead of this ion, they observe $C_{12}H_9O^+$, 4 u greater than $C_{13}H_9^+$, an ion we observe only in very small concentrations. Because we had previously reported $C_{13}H_9^+$ in benzene flames,[27] Löffler and Homann were very careful to confirm the fact that it was not observed.[30] Their instrumentation is better than ours, but it is difficult to see how we could be off in our calibration by 4 u. If we shift our mass scale by 4 u to force a match at 169 u, then our agreement with larger ions falls from 80 ions to 54 ions. Further, we would identify 40 ions which they do not observe and are not observed in the acetylene flame. We thus need to seek elsewhere for this difference in observation of $C_{13}H_9^+$ at mass 165.

One possibility is that the two ions have similar thermodynamic stabilities, so that the differences in our two experiments, Table I, are sufficient to switch the stability from one to the other ion. To determine the feasibility of this would require estimating the thermodynamics for 169 u, which we will do. This ion may also be 152 u with H_2O^+ replacing a H atom or 151 u with H_2O^+ added, but then why does Darmstadt not observe mass 165?

The next step in analyzing the benzene/oxygen flame will be to calibrate the mass spectrometer absolute sensitivity by comparing the mass spectral data with our Langmuir probe data.

XI. PUBLICATIONS AND PRESENTATIONS

1. Keil, D.G. and Calcote, H.F., "Large Ion Formation in a Sooting and Near Sooting Benzene/Oxygen Flame," Fall Technical Meeting, Eastern Section: The Combustion Institute, Orlando, FL, 3-5 December 1990.

2. Calcote, H. F. and Gill, R. J., "Formation of Large Species in Sooting Flames by Free Radical and Ionic Mechanisms," Fall Technical Meeting, Eastern Section: The Combustion Institute, Orlando, FL, 3-5 December 1990.

3. Calcote, H.F., "The Role of Ions in Soot Formation," presented at International Workshop, Mechanisms and Models of Soot Formation, Ruprecht-Karls-Universitat, Heidelberg, Germany, 29 September-2 October 1991.

4. Calcote, H.F. and Gill, R.G., "Comparison of the Ionic Mechanism of Soot Formation with a Free Radical Mechanism," to be published in Proceedings International Workshop, Mechanisms and Models of Soot Formation, Ruprecht-Karls-Universitat, Heidelberg, Germany, 29 September-2 October 1991, Springer-Verlag.

5. Gill, R.J. and Calcote, H.F., "Thermodynamic Properties of Organic Cations," December 1991, submitted to J. Phys. Chem. Ref. Data.

XII. PROFESSIONAL PARTICIPATION

The Principal Investigator on the program is H.F. Calcote who has been responsible for developing the reaction mechanism and collecting the reaction kinetics data. Dr. C.H. Berman extended the Langevin theory to large molecular ions. Dr. Fokian Egolfopoulos modified the Sandia Flame Code to handle ions. Dr. R.J. Gill has been responsible for collecting and calculating the thermodynamics data and for running the modified Sandia Flame Code. The benzene flame experimental data were previously collected by Dr. D.G. Keil who has assisted in reducing them in preparation for modeling. Leslie Van Hoose and J.E. Palmer have assisted with detailed calculations and Helen Rothschild has assisted with graphics and editing. We all acknowledge fruitful discussions with Dr. W. Felder.

XIII. INVENTIONS

None.

XIV. NOMENCLATURE

a_d	=	radius of a disk
a_i	=	hard sphere neutral radius
a_s	=	radius of a sphere
b	=	impact parameter, minimum center to center distance between two molecules if field forces did not affect their trajectories
E	=	electric field strength
E_n	=	electric field strength at the location of the neutral reactant
h	=	thickness of a disk
k	=	collision rate coefficient
n	=	total number density
n_v	=	number of neutral reactant mole molecules having a given velocity v
q_i	=	electric charge on ion
q_p	=	point electrical charge
r	=	distance measured from the center of the ion
r_c	=	critical radius, r, in Langevin theory for which neutral species describes an orbital motion around the ion. Collision occurs when $r < r_c$
r_{min}	=	minimum separation distance between ion and neutral, measured from the center of the ion
r_s	=	separation distance from center of ion to center of molecule at which the electric field strength approaches infinity
v_m	=	mean molecular velocity
v_∞	=	molecular velocity of neutral reactant uninfluenced by the ion
x	=	distance from center of sphere to point where field is measured
y	=	distance from center of sphere to the external point charge
γ	=	polarizability
γ_i	=	polarizability of ion
γ_n	=	polarizability of neutral
$\dot{\theta}$	=	angular rate for neutral molecule orbiting ion
μ	=	reduced mass
$\dot{\theta}$	=	angular rate for neutral molecule orbiting ion

XV. REFERENCES

1. Calcote, H.F. and Gill, R.J., "Computer Modeling of Soot Formation Comparing Free Radical and Ionic Mechanisms," Final Report, AeroChem TP-495, February 1991.

2. Frenklach, M. and Wang, H., "Computer Modeling of Soot Formation Comparing Free Radical and Ionic Mechanisms," Final Report, January 1991.

3. Gill, R.J. and Calcote, H.F., "Thermodynamic Properties of Organic Cations," December 1991, submitted to J. Phys. Chem. Ref. Data.

4. Calcote, H.F., "The Role of Ions in Soot Formation," presented at International Workshop, Mechanisms and Models of Soot Formation, Ruprecht-Karls-Universitat, Heidelberg, Germany, 29 September-2 October 1991; Calcote, H.F. and Gill, R.G., "Comparison of the Ionic Mechanism of Soot Formation with a Free Radical Mechanism," to be published in Proceedings International Workshop, Mechanisms and Models of Soot Formation, Springer-Verlag.

5. Calcote, H.F. and Keil, D.G., "The Role of Ions in Soot Formation," Pure & Appl. Chem. 62, 815-824 (1990).

6. Calcote, H.F. and Keil, D.G., "Ionic Mechanisms of Soot Formation in Flames," Final Report, AeroChem TP-465, June 1987.

7. Langevin, P., Ann. Chim. Phys. 5, 245 (1905).

8. Bei, H.C., Bhowmik, P.K. and Su, T., "Trajectory Calculations of High Temperature and Kinetic Energy Dependent Ion-Polar Molecule Collision Rate Constants," J. Chem. Phys. 90, 7046 (1989).

9. Hirschfelder, J.O., Curtiss, C.F., and Bird, R.B., Molecular Theory of Gases and Liquids (Wiley, New York, 1954).

10. Jackson, J.D., Classical Electrodynamics (Wiley & Sons, New York, 1962).

11. Hinchliffe, A., Munn, W., and Siebrand, W., "Polarizability of Aromatic Hydrocarbon Ions," J. Phys. Chem. 87, 3837 (1983).

12. Morse, P.M. and Feshbach, H., Methods of Theoretical Physics, Part II (McGraw-Hill, New York, 1953).

13. "Soot Formation in Combustion," An International Round Table Discussion, Section IV, "Comparison of Soot Formation in Pyrolysis, Premixed and Diffusion Flames," led by I. Glassman and Discussion, Vandenhoeck and Ruprecht in Göttingen, July 1990, pp. 67-119.

14. Calcote, H.F., Olson, D.B., and Keil, D.G., "Are Ions Important in Soot Formation?" Energy & Fuels 2, 494 (1988).

15. Gerhardt, P.H. and Homann, K.H., "Ions and Charged Soot Particles in Hydrocarbon Flames. I. Nozzle Beam Sampling: Velocity, Energy, and Mass Analysis; Total Ion Concentrations," Combust. Flame 81, 289 (1990).

16. Calcote, H.F., "Ionic Mechanisms of Soot Formation," in Soot in Combustion Systems and Its Toxic Properties, J. Lahaye and G. Prado, Eds. (Plenum Press, New York, 1983) pp. 197-215.

17. Homann, K.H., International Workshop, Mechanisms and Models of Soot Formation, Ruprecht-Karls-Universitat, Heidelberg, Germany, 29 September-2 October 1991

18. Calcote, H.F., "Mechanisms of Soot Nucleation in Flames - A Critical Review," Combust. Flame 42, 215-242 (1981).

19. Gerhardt, P.H. and Homann, K.H., "Ions and Charged Soot Particles in Hydrocarbon Flames. 2. Positive Aliphatic and Aromatic Ions in Ethylene/Oxygen Flames," J. Phys. Chem. 94, 5381 (1990).

20. Gerhardt, P.H.,"Massenspektrometrie Positiver und Negativer Ionen in Brennstofffreichen Ethin-Sauerstoff-Flammen," Dissertation, Technischen Hochschule Darmstadt, 1988.

21. Michaud, P., Delfau, J.L., and Barrassin, A., "The Positive Ion Chemistry in the Post Combustion Zone of Sooting Premixed Acetylene Low Pressure Flat Flames," Eighteenth Symposium (International) on Combustion (The Combustion Institute, Pittsburgh, 1981) p. 443.

22. Bittner, J.D. and Howard, J.B., "Pre-particle Chemistry in Soot Formation," in Particulate Carbon: Formation During Combustion, D.G. Siegla and G.W. Smith, eds. (Plenum, New York, 1981) p. 109.

23. Vovelle, C., personal communications, December 1989 and July 1990.

24. Keil, D.G. and Calcote, H.F., "Large Ion Formation in a Sooting and Near Sooting Benzene/Oxygen Flame," Fall Technical Meeting, Eastern Section: The Combustion Institute, Orlando, FL, 3-5 December 1990.

25. Löffler, S. and Homann, K.H., "Large Ions in Premixed Benzene-Oxygen Flames," Twenty-Third Symposium (International) on Combustion (The Combustion Institute, Pittsburgh, 1991) p. 355.

26. Löffler, S., "Polyeder-Kohlerstaff-und Andere Interessante Ionen in Benzolsauerstaft Flammen," Dissertation, Technischen Hochschule Darmstadt, 1990.

27. Olson, D.B. and Calcote, H.F., "Ions in Fuel-Rich and Sooting Acetylene and Benzene Flames," Eighteenth Symposium (International) on Combustion (The Combustion Institute, Pittsburgh, 1981) p. 453.

28. Homann, K.H., personal communication, September 1991.

29. Stein, S.E., "Structure and Equilibria of Polyaromatic Flame Ions," Combust. Flame 51, 357 (1983).

30. Homann, K.H., personal communication, March 1991.

TABLE I

COMPARISON OF BENZENE/OXYGEN FLAMES OBSERVED AT AEROCHEM AND AT DARMSTADT

	AeroChem	Darmstadt
Equivalence Ratio	1.8, 2.0 + 30 mol% argon	1.9, 2.0
Unburned Gas Velocity, cm s^{-1}	50	42
Pressure, kPa	2.67	2.67
Threshold Soot Formation, ϕ	1.90	1.83
Temperature Peak, K:	1900	2094
at mm above burner:	12.9	11.6
for equivalence ratio:	1.80	1.95

TABLE II

COMPARISON OF IONS OBSERVED IN ACETYLENE/OXYGEN AND BENZENE/OXYGEN FLAMES AND IONS OBSERVED AT AEROCHEM AND AT HOMANN'S LABORATORY IN DARMSTADT, GERMANY

ION MASS	ION FORMULA	ACETYLENE/OXYGEN AERO[a]	ACETYLENE/OXYGEN DARMS[b]	BENZENE/OXYGEN AERO[c]	BENZENE/OXYGEN DARMS[d]
19	H_3O^+			X	
24	C_2^+			X	X
31	CH_3O^+		X		
33	CH_5O^+		X		
39	$C_3H_3^+$	X	X	X	X
41	C_2HO			X	X
43	$C_2H_3O^+$		X	X	X
47	$C_2H_7O^+$		X		
49	C_4H^+				X
51	$C_4H_3^+$		X	X	X
53	$C_4H_5^+$	X	X	X	X
55	$C_3H_3O^+$		X		
57	$C_4H_9^+$, $C_2H_7O^+$			X	X
63	$C_5H_3^+$	X	X	X	X
65	$C_5H_5^+$		X	X	
67	$C_4H_3O^+$		X	X	X
69	$C_4H_5O^+$		X		
71	$C_3H_3^+ \cdot O_2$		X		
73	C_6H^+, $C_4H_9O^+$		X		X
75	$C_6H_3^+$		X	X	X
77	$C_6H_5^+$	X	X	X	
79	$C_6H_7^+$		X	X	X
81	$C_5H_5O^+$		X	X	X
83	$C_4H_3^+ \cdot O_2$		X		
85	$C_4H_5^+ \cdot O_2$		X		
87	$C_7H_3^+$		X	X	X
89	$C_7H_5^+$	X	X	X	
91	$C_7H_7^+$	X	X	X	X
95	$C_6H_7O^+$		X	X	X

TABLE II (continued)

ION MASS	ION FORMULA	ACETYLENE/OXYGEN AERO[a]	ACETYLENE/OXYGEN DARMS[b]	BENZENE/OXYGEN AERO[c]	BENZENE/OXYGEN DARMS[d]
97	C_8H^+		X		X
99	$C_8H_3^+$		X	X	X
103	$C_8H_7^+$	X	X	X	X
105	$C_7H_5O^+$		X	X	X
109	$C_7H_9O^+$		X	X	X
111	$C_9H_3^+$		X	X	X
115	$C_9H_7^+$	X	X	X	X
117	$C_9H_9^+$			X	X
119	$C_8H_7O^+$		X	X	X
121	$C_8H_9O^+$			X	X
123	$C_8H_{11}O^+$		X	X	X
124	$C_8H_{12}O^+$			X	X
126	$C_{10}H_6^+$			X	X
129	$C_{10}H_9^+$	X	X	X	X
131	$C_9H_70^+$, $C_{10}H_{11}^+$		X	X	X
133	$C_9H_9O^+$			X	X
135	$C_{11}H_3^+$		X		
139	$C_{11}H_7^+$		X	X	
141	$C_{11}H_9^+$	X	X	X	X
143	$C_{10}H_7O^+$		X	X	X
145	$C_{10}H_9O^+$		X	X	X
147	$C_{12}H_3^+$		X		
152	$C_{12}H_8^+$			X	X
153	$C_{12}H_9^+$	X	X	X	
155	$C_{11}H_7O^+$, $C_{12}H_{11}^+$			X	X
157	$C_{11}H_9O^+$			X	X
159	$C_{13}H_3^+$		X		
165	$C_{13}H_9^+$	X	X	X	
169	$C_{12}H_{90}O^+$				X
170	$C_{12}H_{10}O^+$			X	X
171	$C_{14}H_3^+$		X		
177	$C_{14}H_9^+$		X	X	X
179	$C_{14}H_{11}^+$	X		X	
181	$C_{13}H_9O^+$			X	X
183	$C_{15}H_3^+$		X		

TABLE II (continued)

ION MASS	ION FORMULA	ACETYLENE/OXYGEN AERO[a]	ACETYLENE/OXYGEN DARMS[b]	BENZENE/OXYGEN AERO[c]	BENZENE/OXYGEN DARMS[d]
189	$C_{15}H_9^+$		X	X	X
191	$C_{15}H_{11}^+$	X	X	X	
192	$C_{14}H_8O^+$			X	X
193	$C_{14}H_9O^+$			X	X
203	$C_{16}H_{11}^+$	X	X	X	
204	$C_{15}H_8O^+$			X	X
205	$C_{15}H_9O^+$			X	X
215	$C_{17}H_{11}^+$	X	X	X	X
217	$C_{16}H_9O^+$			X	X
219	$C_{16}H_{11}O^+$			X	X
227	$C_{18}H_{11}^+$	X	X	X	X
228	$C_{17}H_8O^+$			X	X
231	$C_{17}H_{11}O^+$			X	X
239	$C_{19}H_{11}^+$	X	X	X	X
240	$C_{18}H_8O^+$			X	X
241	$C_{18}H_9O^+$			X	
243	$C_{18}H_{11}O^+$			X	X
250	$C_{20}H_{10}^+$		X		
251	$C_{20}H_{11}^+$	X	X	X	
253	$C_{19}H_9O^+$			X	X
255	$C_{19}H_{11}O^+$				X
263	$C_{21}H_{11}^+$	X	X	X	X
265	$C_{20}H_9O^+$, $C_{21}H_{13}^+$			X	X
267	$C_{20}H_{11}O^+$, $C_{21}H_{15}^+$				X
276	$C_{22}H_{12}^+$		X		
277	$C_{22}H_{13}^+$	X	X	X	
279	$C_{21}H_{11}O^+$, $C_{22}H_{15}^+$			X	X
287	$C_{23}H_{11}^+$		X		
289	$C_{23}H_{13}^+$	X		X	X
293	$C_{23}H_{13}O^+$			X	X
300	$C_{24}H_{12}^+$		X		
301	$C_{24}H_{13}^+$	X	X	X	X
303	$C_{23}H_{11}O^+$			X	X
313	$C_{25}H_{13}^+$	X	X	X	
317	$C_{24}H_{13}O^+$				X

TABLE II (continued)

ION MASS	ION FORMULA	ACETYLENE/OXYGEN AERO[a]	ACETYLENE/OXYGEN DARMS[b]	BENZENE/OXYGEN AERO[c]	BENZENE/OXYGEN DARMS[d]
324	$C_{26}H_{12}^+$		X		
325	$C_{26}H_{13}^+$	X	X	X	
329	$C_{25}H_{13}O^+$				X
337	$C_{27}H_{13}^+$	X	X	X	
341	$C_{26}H_{13}O^+$				X
348	$C_{28}H_{12}^+$		X		
349	$C_{28}H_{13}^+$		X		
350	$C_{28}H_{14}^+$		X		
351	$C_{28}H_{15}^+$		X	X	X
353	$C_{27}H_{13}O^+$				X
361	$C_{29}H_{13}^+$	X	X	X	X
363	$C_{28}H_{11}O^+$		X	X	X
365	$C_{28}H_{13}O^+$			X	X
374	$C_{30}H_{14}^+$		X		
375	$C_{30}H_{15}^+$	X		X	
377	$C_{29}H_{13}O^+$		X		X
385	$C_{31}H_{13}^+$		X		
386	$C_{31}H_{14}^+$			X	X
387	$C_{31}H_{15}^+$	X		X	
391	$C_{30}H_{15}O^+$				X
398	$C_{32}H_{14}^+$		X		
399	$C_{32}H_{15}^+$	X	X	X	
403	$C_{31}H_{15}O^+$				X
411	$C_{33}H_{15}^+$	X	X	X	X
415	$C_{32}H_{15}O^+$				X
422	$C_{34}H_{14}^+$		X		
423	$C_{34}H_{15}^+$	X	X	X	X
427	$C_{33}H_{15}O^+$				X
435	$C_{35}H_{15}^+$	X	X	X	X
439	$C_{34}H_{15}O^+$				X
446	$C_{36}H_{14}^+$		X		
447	$C_{36}H_{15}^+$	X	X	X	X
459	$C_{37}H_{15}^+$	X	X	X	X
470	$C_{38}H_{14}^+$		X		
471	$C_{38}H_{15}^+$	X	X	X	

TABLE II (continued)

ION MASS	ION FORMULA	ACETYLENE/OXYGEN AERO[a]	ACETYLENE/OXYGEN DARMS[b]	BENZENE/OXYGEN AERO[c]	BENZENE/OXYGEN DARMS[d]
472	$C_{38}H_{16}^+$		X		
473	$C_{38}H_{17}^+$			X	X
483	$C_{39}H_{15}^+$	X	X	X	X
497	$C_{40}H_{17}^+$			X	
502	$C_{41}H_{15}^+$		X		
506	$C_{41}H_{15}^+$			X	X
507	$C_{41}H_{15}^+$		X		
508	$C_{41}H_{16}^+$			X	X
509	$C_{41}H_{17}^+$	X		X	X
520	$C_{42}H_{16}^+$		X		
521	$C_{42}H_{17}^+$	X		X	X
533	$C_{43}H_{17}^+$	X	X	X	X
544	$C_{44}H_{16}^+$		X		
545	$C_{44}H_{17}^+$	X	X	X	X
557	$C_{45}H_{17}^+$	X	X	X	X
568	$C_{46}H_{16}^+$		X		
569	$C_{46}H_{17}^+$		X		
581	$C_{47}H_{17}^+$		X		

[a]AeroChem, Ref. 27.

[b]Darmstadt, Refs. 19, 28.

[c]This work.

[d]Refs. 25, 26.

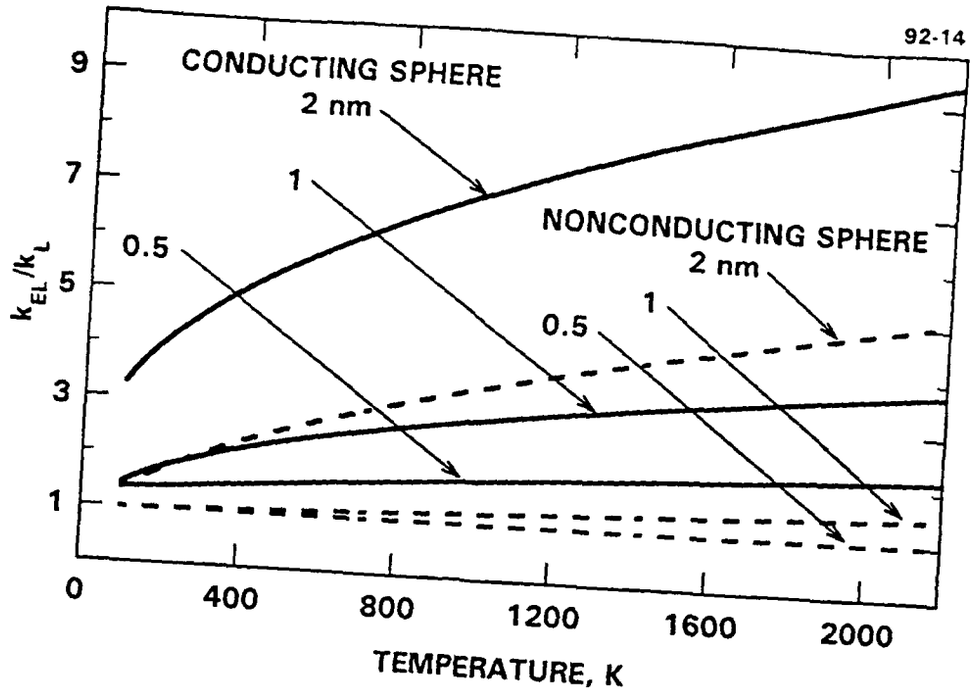

FIGURE 1 RATIO OF EXPANDED LANGEVIN TO LANGEVIN COLLISION RATE
Assumes acetylene as neutral reactant and a single charge on sphere

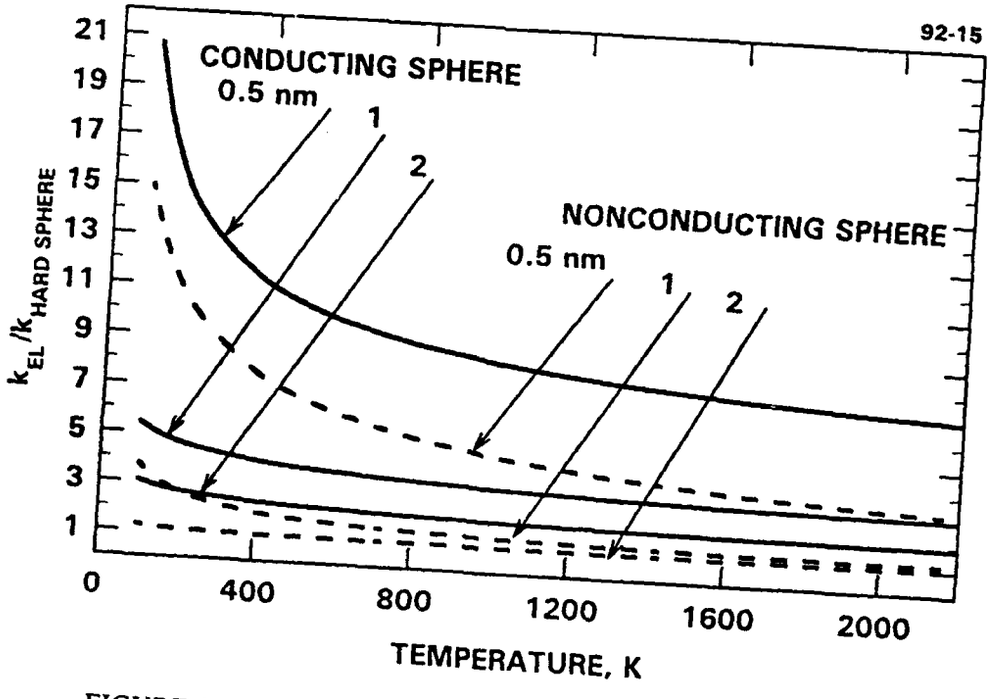

FIGURE 2 RATIO OF EXPANDED LANGEVIN COLLISION RATE TO HARD SPHERE COLLISION RATE
Assumes acetylene as neutral reactant and a single charge on sphere

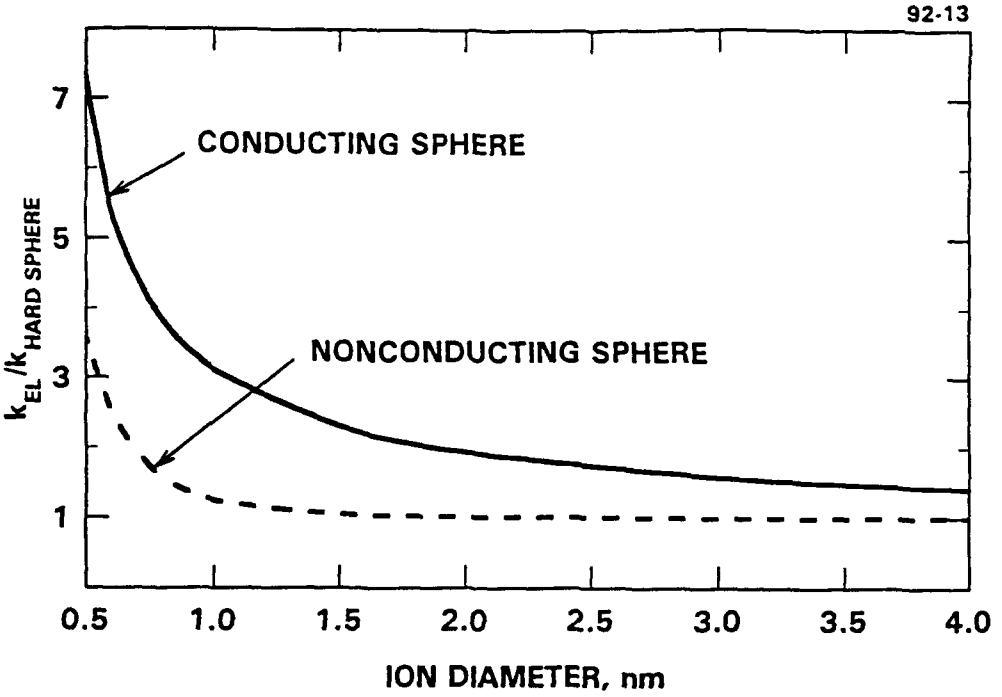

FIGURE 3 EFFECT OF ION DIAMETER ON THE RATIO OF THE EXPANDED LANGEVIN TO THE HARD SPHERE COLLISION RATE
Assumes acetylene as the neutral reactant
and a *single charge on sphere*

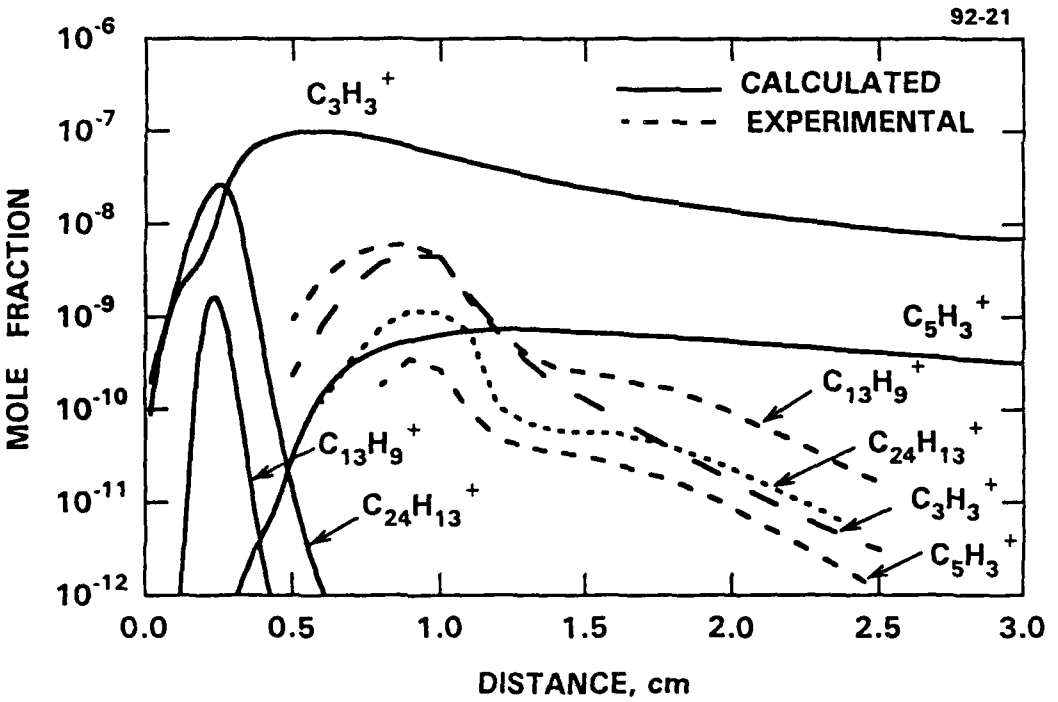

FIGURE 4 COMPARISON OF EXPERIMENTAL WITH CALCULATED ION PROFILES FROM LAST RUN BY FRENKLACH AND WANG

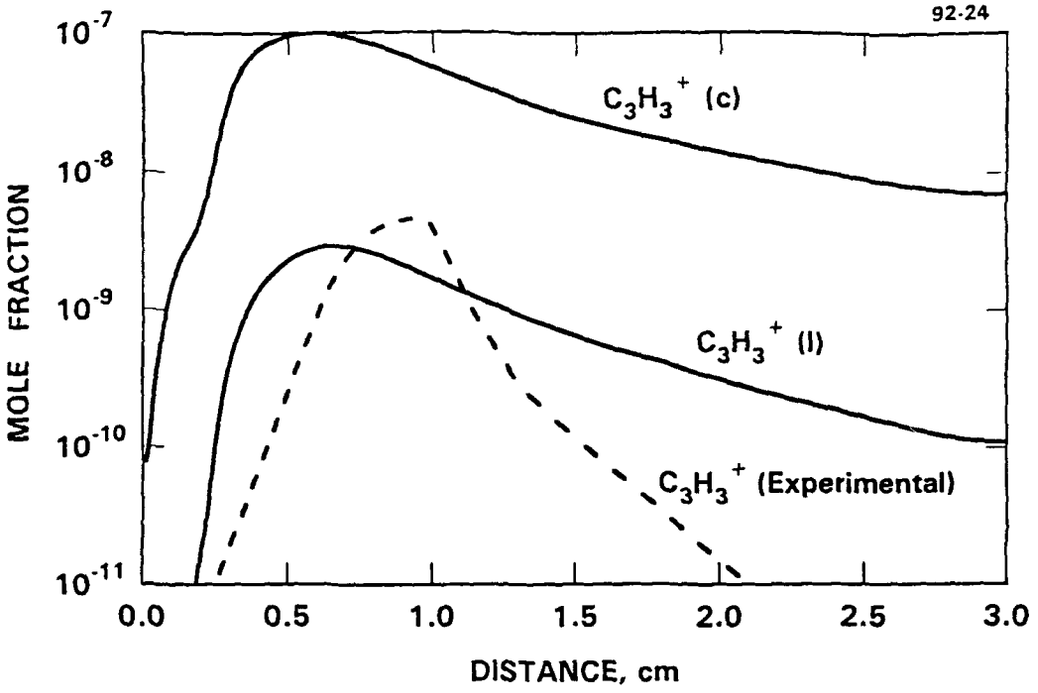

FIGURE 5 COMPARISON OF EXPERIMENTAL SPECIES PROFILES USED AS INPUT DATA TO THE MODIFIED FLAME CODE WITH CALCULATED VALUES FROM LAST RUN BY FRENKLACH AND WANG

——— Calculated; – – – – – – – Experimental

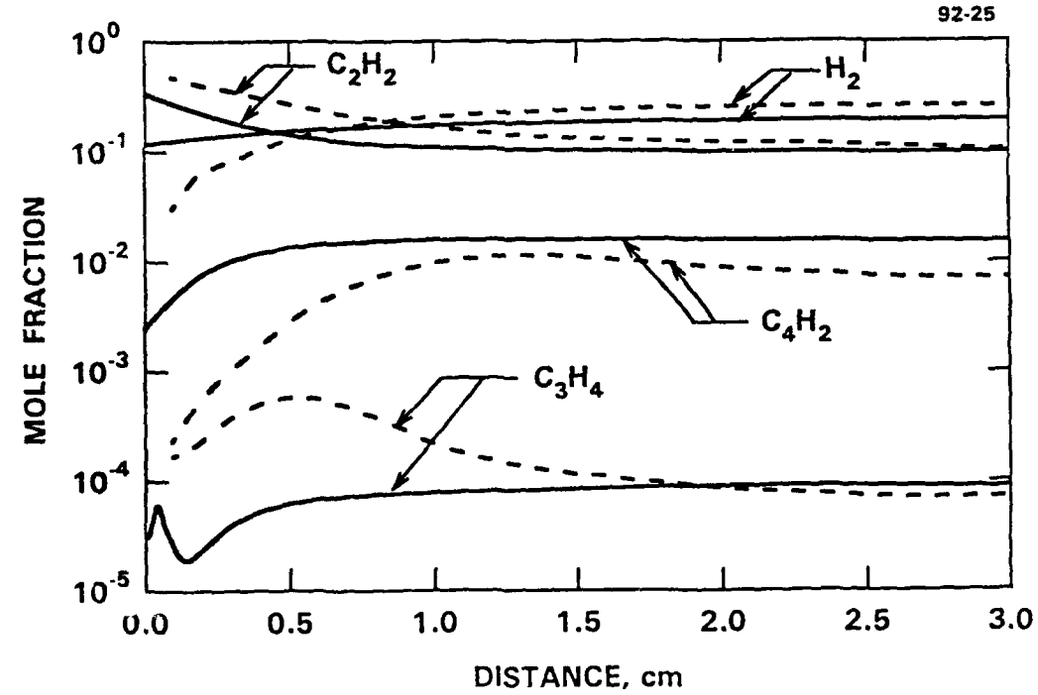

FIGURE 6 COMPARISON OF EXPERIMENTAL SPECIES PROFILES USED AS INPUT DATA TO THE MODIFIED FLAME CODE WITH CALCULATED VALUES FROM LAST RUN BY FRENKLACH AND WANG

——— Calculated; – – – – – – – Experimental

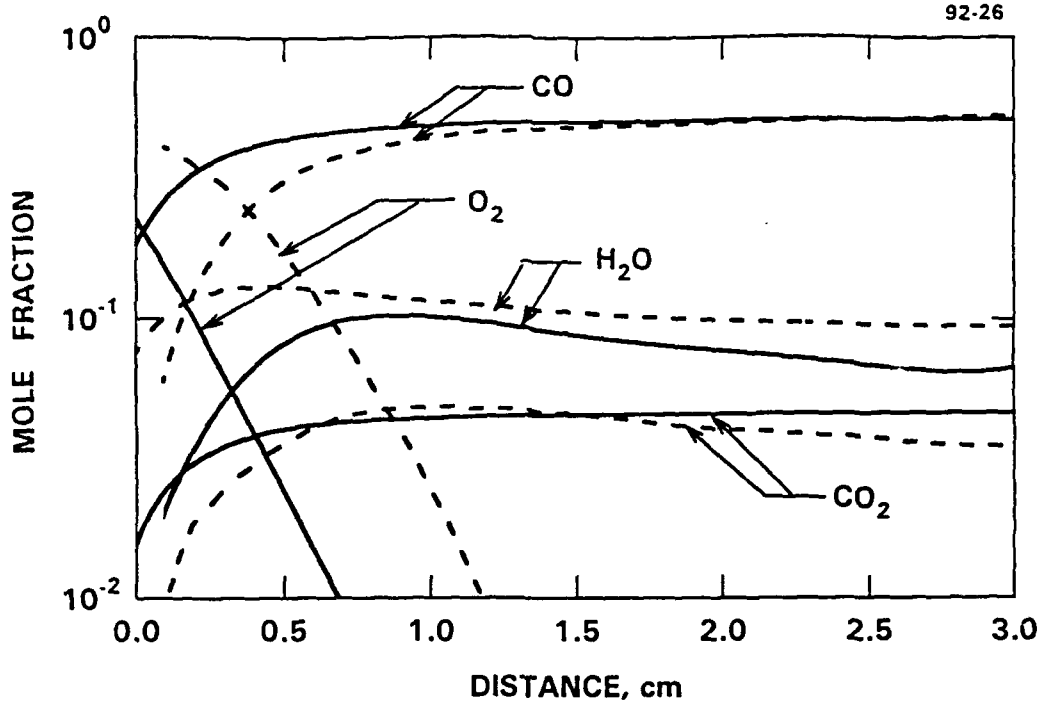

FIGURE 7 COMPARISON OF EXPERIMENTAL SPECIES PROFILES USED AS INPUT DATA TO THE MODIFIED FLAME CODE WITH CALCULATED VALUES FROM LAST RUN BY FRENKLACH AND WANG
——— Calculated; – – – – – – Experimental

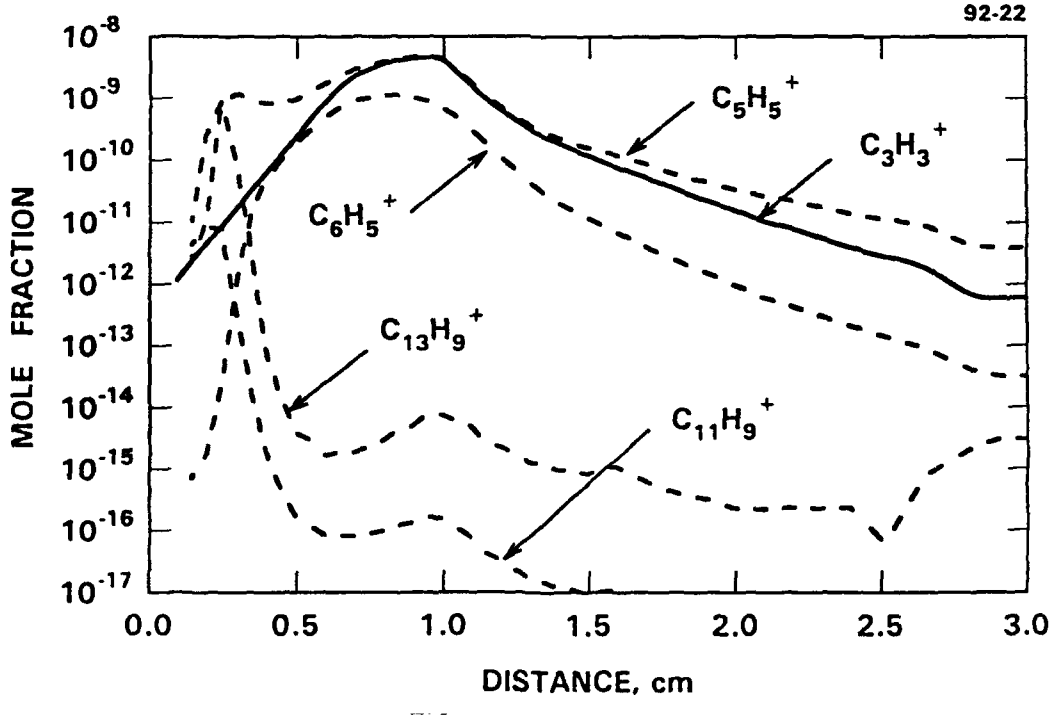

FIGURE 8 TYPICAL CALCULATED ION PROFILES USING THE MODIFIED FLAME CODE

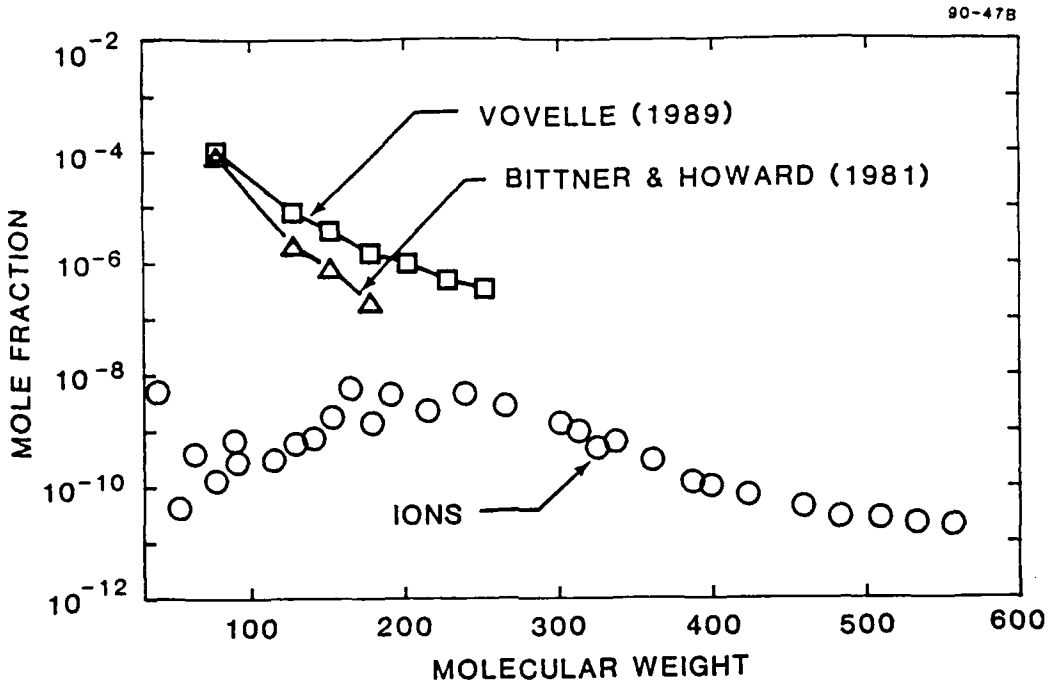

FIGURE 9 RATE OF DECAY OF NEUTRAL AND IONIC SPECIES CONCENTRATION IN ACETYLENE/OXYGEN FLAMES AT 2.67 kPa AND AN EQUIVALENCE RATIO OF 3.0

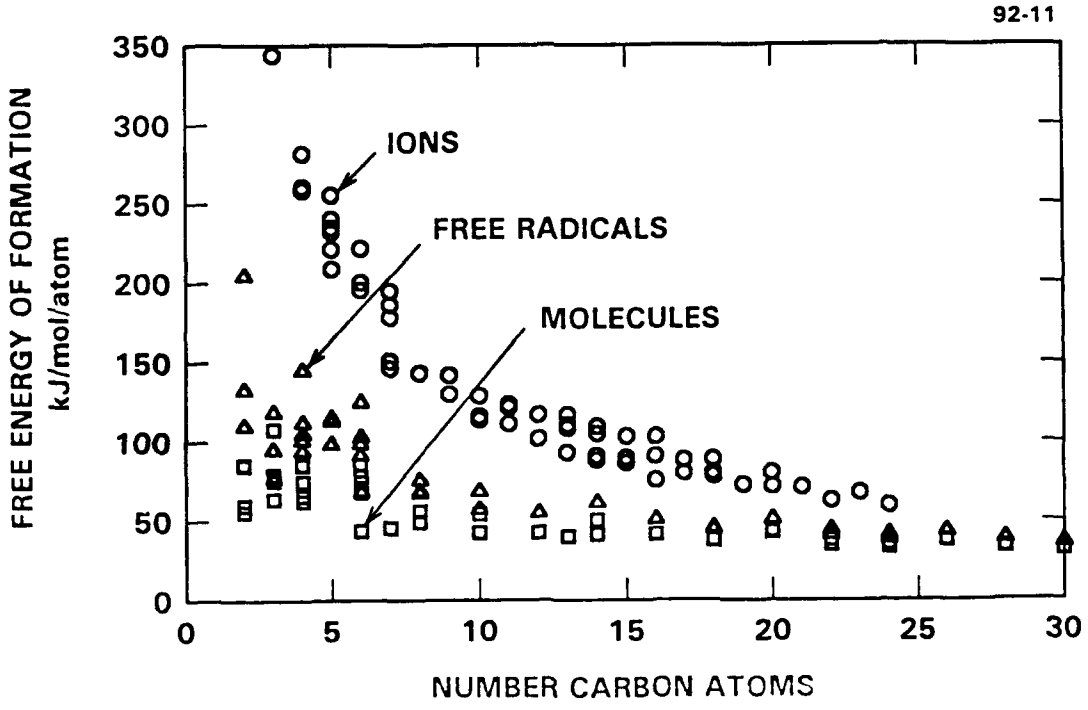

FIGURE 10 FREE ENERGY OF FORMATION PER CARBON ATOM FOR IONS, FREE RADICALS AND MOLECULES AT 1000 K

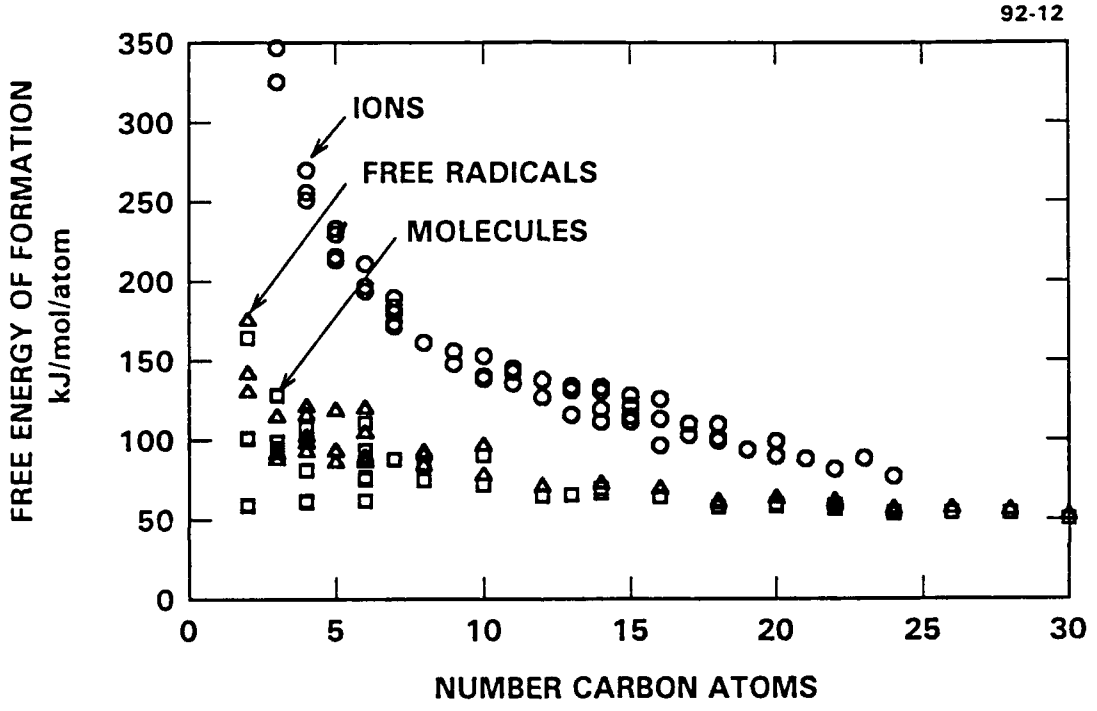

FIGURE 11 FREE ENERGY OF FORMATION PER CARBON ATOM FOR IONS, FREE RADICALS AND MOLECULES AT 2000 K